Title
APOE genotype-dependent pharmacogenetic responses to rapamycin for preventing Alzheimer's disease

Authors
Lin, Ai-Ling
Parikh, Ishita
Yanckello, Lucille M
et al.

Publication Date
2020-06-01

DOI
10.1016/j.nbd.2020.104834

Peer reviewed

HHS Public Access

Author manuscript

Neurobiol Dis. Author manuscript; available in PMC 2020 September 12.

Published in final edited form as:

Neurobiol Dis. 2020 June ; 139: 104834. doi:10.1016/j.nbd.2020.104834.

APOE Genotype-Dependent Pharmacogenetic Responses to Rapamycin for Preventing Alzheimer's Disease

Ai-Ling Lin[1,2,3,4,*], **Ishita Parikh**[1,5], **Lucille M. Yanckello**[1,2], **Renee S. White**[1,6], **Anika M.S. Hartz**[1,2], **Chase E. Taylor**[1], **Scott D. McCulloch**[7], **Scott W. Thalman**[1,4], **Mengfan Xia**[2], **Katie McCarty**[1], **Margo Ubele**[1], **Elizabeth Head**[8,9], **Fahmeed Hyder**[10,11,12,13], **Basavaraju G. Sanganahalli**[10,11,12,13]

[1]Sanders-Brown Center on Aging, University of Kentucky, Lexington, KY

[2]Department of Pharmacology and Nutritional Science, University of Kentucky, Lexington, KY

[3]Department of Neuroscience, University of Kentucky, Lexington, KY

[4]F. Joseph Halcomb III, Department of Biomedical Engineering, University of Kentucky, Lexington, KY

[5]Oklahoma Medical Research Foundation, Oklahoma City, OK

[6]Georgetown College, Georgetown, KY

[7]Metabolon Inc., Durham, NC

[8]Department of Pathology & Laboratory Medicine, University of California, Irvine, CA

[9]University of California Irvine Institute for Memory Impairments and Neurological Disorders, Irvine, CA

[10]Magnetic Resonance Research Center, Yale University, New Haven, CT

[11]Quantitative Neuroscience with Magnetic Resonance Core Center, Yale University, New Haven, CT

[12]Department of Diagnostic Radiology, Yale University, New Haven, CT

[13]Department of Biomedical Engineering, Yale University, New Haven, CT

Abstract

The *ε4* allele of Apolipoprotein (APOE4) is the strongest genetic risk factor for Alzheimer's disease (AD), the most common form of dementia. Cognitively normal APOE4 carriers have developed amyloid beta (Aβ) plaques and cerebrovascular, metabolic and structural deficits decades before showing the cognitive impairment. Interventions that can inhibit Aβ retention and restore the brain functions to normal would be critical to prevent AD for the asymptomatic APOE4 carriers. A major goal of the study was to identify the potential usefulness of rapamycin (Rapa), a pharmacological intervention for extending longevity, for preventing AD in the mice that express human APOE4 gene and overexpress Aβ (the E4FAD mice). Another goal of the study was to

[*]Correspondence: Ai-Ling Lin, Ph.D., Sanders-Brown Center on Aging, University of Kentucky, 800 S. Limestone Street, Lexington KY 40536-0230, ailing.lin@uky.edu.

identify the potential pharmacogenetic differences in response to rapamycin between the E4FAD and E3FAD mice, the mice with human *APOE ε3* allele. We used multi-modal MRI to measure *in vivo* cerebral blood flow (CBF), neurotransmitter levels, white matter integrity, water content, cerebrovascular reactivity (CVR) and somatosensory response; used behavioral assessments to determine cognitive function; used biochemistry assays to determine Aβ retention and blood-brain barrier (BBB) functions; and used metabolomics to identify brain metabolic changes. We found that in the E4FAD mice, rapamycin normalized bodyweight, restored CBF (especially in female), BBB activity for Aβ transport, neurotransmitter levels, neuronal integrity and free fatty acid level, and reduced Aβ retention, which were not observe in the E3FAD-Rapa mice. In contrast, E3FAD-Rapa mice had lower CVR responses, lower anxiety and reduced glycolysis in the brain, which were not seen in the E4FAD-Rapa mice. Further, rapamycin appeared to normalize lipid-associated metabolism in the E4FAD mice, while slowed overall glucose-associated metabolism in the E3FAD mice. Finally, rapamycin enhanced overall water content, water diffusion in white matter, and spatial memory in both E3FAD and E4FAD mice, but did not impact the somatosensory responses under hindpaw stimulation. Our findings indicated that rapamycin was able to restore brain functions and reduce AD risk for young, asymptomatic E4FAD mice, and there were pharmacogenetic differences between the E3FAD and E4FAD mice. As the multi-modal MRI methods used in the study are readily to be used in humans and rapamycin is FDA-approved, our results may pave a way for future clinical testing of the pharmacogenetic responses in humans with different APOE alleles, and potentially using rapamycin to prevent AD for asymptomatic APOE4 carriers.

Keywords

APOE4; APOE3; Alzheimer’s disease prevention; Rapamycin; mTOR; MRI; pharmacogentics; cerebral blood flow; cerebrometabolic function; white matter integrity; blood brain barrier; amyloid-beta plaques; cognition; cerebrovascular reactivity; water content; neuroinflammation

Introduction

Alzheimer’s disease (AD) is the most common form of dementia with hallmarks of amyloid beta (Aβ) plaques and neurofibrillary tau tangles (NFT) [1, 2]. The strongest genetic risk factor for late onset AD is the presence of the *ε4* allele of Apolipoprotein (APOE4) [3]. Individuals with APOE4 gene are 3 (heterozygous) - to 15 (homozygous) - fold more likely to have late-onset AD compared to the non-carriers [4, 5]. Several decades before the possible onset of dementia, cognitively normal APOE4 carriers have developed abnormal brain glucose uptake as detected by in vivo positron emission tomography (PET) imaging [3, 6–9]. Using magnetic resonance imaging (MRI), a recent study showed that asymptomatic APOE4 carriers have altered cerebral blood flow (CBF) [10], and longitudinal studies have shown that CBF is reduced in an accelerated manner in cognitively healthy APOE4 carriers [6]. The neurovascular risk is highly associated with accelerated decline in language ability, verbal memory, attention, and visuospatial abilities in midlife of the APOE4 carriers [11]. Metabolic and vascular impairments can lead to brain structural damage (e.g., due to oxidative stress and reduced nutrient supply). In line with this, MRI-based diffusion tensor imaging (DTI) studies have found that white matter (WM) integrity is compromised in

healthy APOE4 carriers [12, 13]. These neuroimaging findings indicate that brain physiology and structure are altered in APOE4 carriers before clinical markers such as Aβ and NFT pathology, and memory deficits appear; Aβ deposition later in life would interact with APOE4 to promote further cognitive decline [14]. Therefore, early intervention to restore brain metabolic, vascular, and anatomical integrity may be critical for reducing the risk of cognitive impairment later in life among APOE4 carriers.

We have previously shown that rapamycin, a pharmacological intervention for extending longevity, was able to protect brain functions of the asymptomatic APOE4 transgenic mice [15, 16]. Rapamycin is an inhibitor of the mechanistic target of rapamycin (mTOR) signaling pathway. Evidence from postmortem human AD brains indicates that the levels of phospho-mTOR are increased compared to age-matched control cases, suggesting higher mTOR activity in AD brains [17, 18]. In contrast, mTOR inhibition has been shown to prevent neurodegeneration and protect brain functions in aging. Notably, rapamycin reduces Aβ and NFT and improves cognitive functions in mice that model human AD [19, 20].

We have shown that rapamycin was able to restore brain glucose uptake, CBF and blood-brain barrier (BBB) integrity in the young APOE4 transgenic mice; the preserved vascular and metabolic functions were associated with amelioration of incipient learning deficits of the APOE4 transgenic mice [15, 16]. The results from the study suggested that rapamycin might have a protective effect on brain physiological functions and potentially prevent AD for APOE4 carriers. However, as the APOE4 transgenic mice used in the study do not generate Aβ or NFT, the physiology and pathology observed in the mouse model may not fully reflect that of human AD.

In this study, we used an advanced mouse model that overexpresses human Aβ via 5 familial-AD (5xFAD) mutations, and expresses human APOE4, known as the E4FAD mice [21]. We compared the results with mice having the more common *APOE ε3* genotype (E3FAD), which is considered risk-neutral for AD. It has been shown that in this model, Aβ initiated at 4 months in the subiculum and deep layers of the frontal cortex and is increased by 6 months regardless APOE genotypes. Aβ plaque deposition was greater in E4FAD mice compared with E3FAD mice and was significant at 4 months in the frontal cortex and subiculum and at 6 months in the frontal cortex [22].

Using the model will allow us further to identify the effectiveness of rapamycin for preventing Aβ aggregation and AD progression. A major goal of the study is to determine if we treated the E4FAD mice with rapamycin before they develop Aβ, whether the brain physiological, structural, and cognitive functions can be preserved and Aβ accumulations can also be prevented. We fed the mice with rapamycin from 3 months of age (before they developed significant Aβ retention) and continued for 16 weeks. We used multimodal MRI methods to determine *in vivo* vascular, metabolic and structural (WM) functions. We used behavioral tests to assess cognitive functions, employed biochemical assays to measure BBB function and Aβ retention, and used metabolomics to determine changes in metabolic pathways of the brain. We hypothesized that rapamycin would restore brain vascular, metabolic, structural integrity, enhance Aβ clearance and protect cognitive functions of the pre-symptomatic E4FAD mice.

Another major goal of the study is to identify the potential pharmacogenetic differences in response to rapamycin between the E4FAD and E3FAD mice. It is critical to know if the responses to rapamycin would be APOE genotype- dependent. The findings from the current study may provide important information in regard to preventing AD with precision medicine in the future.

Materials and Methods

Animals and Experimental Design

We used a C57BL/6 mouse model which accumulates human $A\beta_{42}$ due to co-expression of 5 familial-AD (5xFAD) mutations (APP K670N/M671L+I716V+V717I and PS1 M1461L +L286V) in conjunction with human targeted replacement *APOE* (*ε4* in the *E4*FAD line and *ε3* in the *E3*FAD line). We originally obtained the breeders from Dr. Mary Jo LaDu of the University of Illinois at Chicago [21], and have established our own colony at the University of Kentucky. Each mouse was genotyped to verify their *APOE* and FAD genotype via Transnetyx Inc. (Cordova, TN, USA) after weaning. We determined the sample size (N = 5–18/group) via power analysis to ensure comparison at a 0.05 level of significance and 90% chance of detecting a true difference of each measured variable between the groups. We had compariable number of male and female mice in each experiment (Table 1). The mice were randomized and assigned into the following groups: (i) E3FAD-Rapa and E4FAD-Rapa — mice fed with rapamycin supplemented diet or (ii) E3FAD-Control and E4FAD-Control — mice fed with control diet (same nutritional ingredient composition and proportion), started from 3 months of age and continued for 16 weeks. Rapamycin is at 14mg per kg (ppm) food, which is approximately equivalent to 2.24mg/kg/mouse/day based on the assumption that an average mouse weighs 30g and consumes 5g of food per day. The diets were prepared by TestDiets after analysis. Mice were fed ad libitum and weighed bi-weekly. At the end of the study, we found that the E4FAD mice had a higher body weight (39.5 ± 6.6 gm) compared to their E3FAD littermates (26.7 ± 2.5 gm) ($p < 0.01$), and rapamycin normalized the bodyweight of the E4FAD mice to a level similar to the E3FAD-Rapa mice (E4FAD vs E3FAD: 35.6 ± 9.2 gm vs. 32.4 ± 5.2 gm; $p > 0.5$); no bodyweight difference was found between the E3FAD-Cotnrol and E3FAD-Rapa mice. All experimental procedures were performed according to NIH guidelines and approved by the Institutional Animal Care and Use Committee (IACUC) at the University of Kentucky (UK).

In vivo Neuroimaging

Cerebral Blood Flow (CBF) Measurement—We measured CBF using MRI-based arterial spin labeling (ASL) techniques. Details have been described in a previous study [23]. Briefly, MRI experiments were performed on a 7T MR scanner (Clinscan, Bruker BioSpin, Germany) at the Magnetic Resonance Imaging & Spectroscopy Center of the University of Kentucky. Mice were anesthetized with 4.0% isoflurane for induction and then maintained in a 1.2% isoflurane and air mixture using a nose cone. Heart rate (90–110 bpm), respiration rate (50–80 breaths/min), and rectal temperature (37 ± 1°C) was continuously monitored and maintained. A water bath with circulating water at 45–50°C was used to maintain the body temperature. A whole-body volume coil was used for transmission and a mouse brain surface coil was placed on top of the head for receiving. We measured CBF using MRI-

based pseudo-continuous ASL (pCASL) techniques [23]. Paired control and label images were acquired in an interleaved fashion with a train of Hanning window-shaped radiofrequency pulses of duration/spacing = 200/200 μs, flip angle = 25° and slice-selective gradient = 9 mT/m, and a labeling duration = 2100 ms. The images were acquired by 2D multi-slice spin-echo echo planner imaging with FOV =18 ×18 mm^2, matrix =128 × 128, slice thickness = 1 mm, 10 slices, TR = 4,000 ms, TE = 35 ms, and 120 repetitions. pCASL images were analyzed with in-house written codes in MATLAB (MathWorks, Natick, MA) to obtain quantitative CBF (with units of mL/g per minute). Brain structural T_2-weighted images were acquired with field of view (FOV) =18 ×18 mm^2, matrix = 256 × 256; slice thickness = 1 mm, 10 slices, repetition time (TR) = 1500 ms, and echo time (TE) = 35 ms. The CBF images were then superimposed to the corresponding structural images using Multi-Image Analysis GUI (Mango) software (http://rii.uthscsa.edu/mango/).

Brain Metabolite Measurement—Brain metabolites were determined using proton magnetic resonance spectroscopy (^{1}H-MRS) method with a point-resolved spectroscopy sequence (PRESS) sequence. Water-suppressed spectra were acquired with the following parameters: TR = 1500 ms, TE = 135 ms, spectral width = 60 Hz, and average = 400. A voxel (2.0 mm × 5.0 mm × 1.3 mm) is placed over the bilateral hippocampus. An acquisition of non-water-suppressed spectrum with 10 averages was followed (the rest of the parameters were kept the same). Both of these spectra were processed using the LCModel which included the basis set: alanine (Ala), total choline (TCho), glutamate-glutamine complex (Glu/Gln), myo-inositol (mI), lactate (Lac), N-acetyl aspartate (NAA), phosphocreatine (PCr), total creatine (TCr), and taurine (Tau) [24, 25]. Quantitative concentrations of the metabolites (in micromolar) were computed by $[m] = (S_m/S_{water})[\text{water}]C_nC_{av}$ where $[m]$ is the metabolite concentration, S_m is the metabolite intensity acquired from MRS, S_{water} is the water intensity acquired from MRS, [water] is the concentration of water (55.14mM at 310K), C_n is the correction for the number of equivalent nuclei for each resonance, and C_{av} is the correction for the number of averages.

Water Content Measurement—Brain dehydration is associated with cognitive impairment [26]. The measurement would help us identify the potential usefulness of rapamycin for preserving water concentration in the brain, which can be indexed by the brain-blood partition coefficient (BBPC). Rapid Calibrated Short TR Recovery (CaSTRR) method was used to measure BBPC in mice as previously described [27, 28]. The CaSTRR proton density measurements were acquired using a 39 mm birdcage transmit/receive coil. A series of image stacks was acquired to measure the proton density, using phase-spoiled, fast low-angle shot gradient echo (FLASH-GRE) sequence with varying repetition times (TR = 125, 187, 250, 500, 1000, 2000 ms). The shortest possible echo time (TE = 3.2 ms) was used to minimize T2* decay. Multiple averages were taken for the images with TR = 125 ms (4 averages), 187 ms (4 averages) and 250 ms (2 averages) for better signal countering noise. Image matrix parameters results are as follows: field of view = 2.8 cm × 2.8 cm, matrix = 256 × 256, in-plane resolution = 0.11 mm × 0.11 mm, slice thickness = 1 mm, number of slices = 10, flip angle = 90°, acquisition time = 17 min [29]. BBPC maps were calculated in a voxel-wise manner by first fitting the signal recovery curve to the mono-exponential equation S = M0*[1 –ê(-TR/T1)] to yield a map of M_0. Then, the M_0 map was normalized to

the respective phantom series by fitting a linear regression to the average M_0 value in each phantom. Finally, the proton density in each voxel of the brain was compared to the average proton density of the blood ROI using the equation BBPC $=M_{0,\,brain}/(M_{0,\,blood}* 1.04$ g/mL) [27, 29]. Regions of interest were drawn on the hippocampus manually on each analyzed slice to calculate BBPC values. All analysis was performed with in-house written scripts in MATLAB.

White Matter Integrity Determination—A subset of mice (n = 6 per group) were transferred to Yale University for the white matter integrity determination using DTI methods. The experiments were performed in accordance with protocols approved by the IACUC of Yale University School of Medicine. Animals were anesthetized using intraperitoneal injection of urethane (1.3 mg/kg body weight), then placed in a custom-built frame, where they were freely breathing a mixture of O_2 and N_2O (30/70%) through a nose cone. Body temperature was monitored throughout the procedure using a rectal probe and maintained within 35–37°C using warm water pumped through a pad. MRI data were obtained on a modified 11.7T system with Bruker spectrometer and custom built ^1H surface coil (1.4 cm). Images were acquired over 20 contiguous coronal slices (thickness = 400 um), covering the parenchyma between the olfactory bulb and cerebellum, with an in-plane field of view of 400 × 400 um. Anatomical reference images (TR/TE = 4000/20 ms, 4 averages) were acquired in a 128 × 64 matrix, for an effective in-plane resolution of 200 × 200 μm. T2-weighted datasets were acquired with a 2D fast spin-echo sequence using imaging parameters: TR=6000 ms, number of echoes: 10, echo spacing=10ms, 10 coronal 0.8 mm slices, effective in-plane resolution of 200 × 200 μm. T2-weighted image reconstruction and T2 map calculations were performed using programs written with MATLAB software.

DTI was acquired as a 4-segment echo planner imaging (EPI) in a 128 × 64 matrix (in-plane resolution = 200 × 200 μm), with 5 A_0 images, TR/TE = 4000/20 ms, 4 averages, 20 diffusion directions and a b-value of 1000 s/mm. DTI analyses were performed using BioImage Suite, the tensor model was fitted at every voxel of the diffusion sensitive images to generate parametric maps of fractional anisotropy (FA) and the three eigen values were averaged to obtain apparent mean diffusivity (MD) maps.

Hindpaw Stimulation and Cerebrovascular Reactivity (CVR) Measurements—The study was also conducted at Yale University. Following the DTI experiments, functional MRI (fMRI) data were acquired during hindpaw stimulation and hypercapnic (CO_2) challenge experiments. Two subcutaneously placed copper needles were inserted into the contralateral hindpaw (between the second and fourth digits) and all snout whiskers were shaved to avoid contaminating somatosensory signals. All stimulus presentation was controlled by a μ1401 analog-to-digital converter unit (CED, Cambridge, UK) running a custom-written script for providing block design (off-on-off) electrical stimuli of 30 s in duration to provide 0.3 ms duration monophasic square wave pulses with 0.75 mA amplitude by an isolation unit (WPI, Sarasota, FL). We chose a fixed frequency of 10 Hz where we obtained robust fMRI responses under urethane anesthesia. Functional MRI images using the EPI sequence (TR/TE= 1000/15 ms, preceded by 8 dummy scans) were acquired with the same geometry as DTI: for the resting-state paradigm, each scan lasted for 5 minutes

(300 repetitions), repeated four times per animal; the arterial CO_2 change-induced cerebrovascular reactivity functional scans lasted for 12 minutes (720 repetitions), with 5% CO_2 added to the breathing gas mixture between minutes 3 and 6 of the acquisition, and repeated twice per animal. Lastly, a 3D anatomical scan (TR/TE = 50/5.6 ms, FA = 20°, 2 averages) was acquired with an isotropic resolution of 250 μm, for image registration purposes.

fMRI-based blood oxygenation level dependent (BOLD) signals were subjected to a translational movement criterion using a center-of-mass analysis. If any center-of-mass value in a series deviated by more than 25% of a pixel, the entire dataset was discarded from further analysis. Activation foci for fractional change in BOLD maps were obtained by applying a Student's t-test comparison of resting and stimulated data, where statistically significant t values were generated using a paired t test between baseline and stimulation periods (30s baseline and 30s stim for hindpaw; 3 min baseline and 3 min stim period for CO_2 Challenge). Results displayed as t maps of BOLD activations were superimposed on corresponding anatomical images, with approximate coordinates relative to the bregma. Anatomical images were co-registered between mice as follows: Using BioImage Suite (Yale School of Medicine, 2015, bioimagesuite.yale.edu), mice 2–6's anatomical images were registered to mice 1's anatomical image using a nonlinear registration (50 iterations, normalized mutual information, otherwise default). Then, the average of all six registered images (where data were available) was taken to create a "template" image. All mice anatomical images were then registered to the template using a nonlinear registration (50 iterations, normalized mutual information, and otherwise default). Functional images were co-registered between mice as follows: slice-timing correction followed by motion-correction (to the middle volume rather than the first volume) was performed in SPM8 (The FIL Methods group, 2015, www.fil.ion.ucl.ac.uk/spm/software/spm8). Following this, the corresponding mouse's nonlinear transformation to the template was applied using BioImage Suite. To facilitate inter-animal comparison, data were blurred, per-slice, with a Gaussian filter (σ=2 voxels/0.250mm, size=8 voxels/1mm). Group-level t-statistical maps for each sensory modality were binarized at a threshold corresponding to $p < 0.05$.

Behavioral tests

Novel Object Recognition—The behavioral tests were conducted in the Rodent Behavioral Core (RBC) at the University of Kentucky. Novel Object Recognition (NOR) was used to test spatial recognition memory [30]. This task of recognition memory utilizes the fact that animals will spend more time exploring a novel object compared to an object that they are familiar with in order to satisfy their innate curiosity/exploratory instinct. Mice were given 15 minutes to explore two of the same objects in the "A/A" session. For the 10-minute "A/B" test session, one of the A objects was replaced by a novel object (B). There was a 2-hour delay between the A/A and A/B sessions. The total time mice spend investigating the objects was recorded and scored by the fully automated EthoVision XT 8.0 video tracking software. The D_2 discrimination index was calculated by: $D_2 = (T_B\text{-}T_A) \div (T_B + T_A)$, where T_B is the time spent with the novel object B, and T_A is the time spent with the familiar object A.

Elevated Plus Maze—We used elevated plus maze (EPM) to evaluate anxiety of the mice [23, 31], which was also performed at RBC at the UK. The EPM consists of two open and two closed arms elevated 100 cm above the floor. Open arms are perceived as exploratory zones, and thus mice with lower anxiety had tendency to stay in the open arms. We determined the anxiety-related behavior by measuring the time spent in the open arms over the 5-minute test session by EthoVision XT 8.0 video tracking software.

Biochemistry Assays

P-glycoprotein (P-gp) Transport Determination and Western Blotting

Capillary isolation: BBB function was determined by measuring P-gp transport activity from cortical capillaries. After the neuroimaging and behavioral experiments, mice were sacrificed and brain capillaries were isolated according to a previously described protocol [32, 33]. Briefly, mice were euthanized by CO_2 inhalation and decapitated; brains were immediately harvested and collected in ice-cold DPBS buffer supplemented with 5 mM D-glucose and 1 mM Na-pyruvate, pH 7.4. Brains were dissected by removing meninges, choroid plexus and white matter, and homogenized in DPBS. The brain homogenate was mixed with Ficoll® and centrifuged at 5,800g for 15 min at 4°C. The capillary pellet was resuspended in 1% BSA buffer and first passed through a 300 μm nylon mesh followed by filtration through a 27 μm nylon mesh. Capillaries retained by the 27 μm nylon mesh were collected and washed with DPBS buffer and used for experiments.

P-glycoprotein transport activity: Isolated brain capillaries were incubated for 1 h at room temperature with 2 μM NBD-CSA (custom-synthesized by R. Wenger, Basel, Switzerland) in DPBS buffer. Per treatment group, 10 capillary images were acquired by confocal microscopy (Leica TSP SP5 Confocal Microscope with Environmental Chamber, 63 × D-Water UV objective, numerical aperture 1.2, 488-nm line of an argon laser, Leica Microsystems). Confocal images were analyzed by quantitating luminal NBD-CSA fluorescence with Image J software (v.1.45s; Wayne Rasband, NIH). Specific, luminal NBD-CSA fluorescence was taken as the difference between total luminal fluorescence and fluorescence in the presence of the P-glycoprotein specific inhibitor PSC833 (5 μM, Novartis, Basel, Switzerland). For each measurement, 10 capillaries per group were pooled for analyzed and imaged.

Western blotting and quantification: To determine protein expression, isolated brain capillaries were homogenized in tissue lysis buffer containing protease inhibitor cocktail. Homogenized brain capillary samples were centrifuged at 10,000 g for 15 min at 4°C, followed by centrifugation of the denucleated supernatants at 100,000 g for 90 min at 4°C. Pellets (crude brain capillary plasma membranes) were resuspended and protein concentrations were determined using the Bradford protein assay. Western blots were performed using the NuPage™ electrophoresis and blotting system from Invitrogen (Carlsbad, CA, USA). Blotting membranes were incubated overnight with antibody to P-gp (C219; MA1–26528, ThermoFisher, 1μg/ml) and β-actin (ab8226 from Abcam, 1:1000, 1 μg/ml). Proteins were detected using SuperSignal® West Pico Chemoluminescent substrate (Pierce, Rockford, IL, USA) and protein bands were visualized with a BioRad Gel Doc™ XRS imaging system. Image Lab 5.0 software from Bio-Rad Laboratories was used for

densitometric analyses of band intensities and digital molecular weight analyses; the molecular weight marker was RPN800E (GE Healthcare, Chalfont St. Giles, Buckinghamshire, UK). Linear adjustments of contrast and brightness were applied to entire Western blot images. None of the Western blots shown were modified by nonlinear adjustments. Tissue was pooled tissue and n=3 for technical replicates.

Immunohistochemistry - Amyloid-β Staining—Half hemisphere of the mouse brain was collected upon sacrifice and immediately put into a 10% Neutral Buffered Formalin for 24–48 hours. After this time period, the brains were transferred into 90% ethanol. Next, the brains were sent to the COCVD Pathology Research Core at the University of Kentucky to be embedded and sectioned onto microscope slides for immunohistochemistry. The sectioned tissue undergoes rehydration followed by tissue pretreatment in 90% formic acid for 3 minutes. The tissue was then treated with 3% H_2O_2 and 10% methanol for 30 minutes. Next, a M.O.M. Kit (Vector Laboratories, Inc. Burlingame, CA) was used following the standard protocol. Aβ was identified using an anti-$Aβ_{1–17}$ mouse monoclonal 6E10 antibody (1:3000; Signet Laboratories, Dedham, MA). Following this portion of the protocol, a DAB substrate kit (also Vector Laboratories, Burlingame, CA) was used for visualization. Next, a background stain utilizing NISSL was completed followed by dehydration. The slides were next imaged on the Aperio ScanScope XT Digital Slide Scanner System in the University of Kentucky Alzheimer's Disease Center Neuropathology Core Laboratory (20x magnificantion) and uploaded to the online database. Aperio ImageScope (version 12.3.2.8013) was used to analyze total anti-Aβ counted at 20x magnification (0.495px/um). 10 boxes (ROIs that are 600×600×600 microns) were randomly placed in each sample image and counted for percent positive Aβ (number of positive + number of strong positive/total number).

Metabolomics profiling—The other half hemisphere of brain tissue from each mouse was sent to Metabolon Inc. (Durham, NC) for non-targeted metabolomics as previously described [25, 34]. Metabolon's standard solvent extraction method was used to prepare the samples for analysis via liquid chromatography/mass spectrometry (LC/MS) using their standard protocol [35]. The UPLC/MS/MS portion of the platform incorporates a Waters Acquity UPLC system and a Thermo-Finnegan LTQ mass spectrometer, including an electrospray ionization (ESI) source and linear ion-trap (LIT) mass analyzer. Aliquots of the vacuum-dried sample were reconstituted, one each in acidic or basic LC-compatible solvents containing 8 or more injection standards at fixed concentrations (to both ensure injection and chromatographic consistency). Extracts were loaded onto columns (Waters UPLC BEH C18–2.1 × 100 mm, 1.7 μm) and gradient-eluted with water and 95% methanol containing 0.1% formic acid (acidic extracts) or 6.5 mM ammonium bicarbonate (basic extracts). The instrument was set to scan 99–1000 m/z and alternated between MS and MS/MS scans.

Samples destined for analysis by GC-MS were dried under vacuum desiccation for a minimum of 18 h prior to being derivatized using bis(trimethylsilyl)trifluoroacetamide (BSTFA) as described [36]. Derivatized samples were separated on a 5% phenyl dimethyl silicone column with helium as carrier gas and a temperature ramp from 60° to 340°C within a 17-min period. All samples were analyzed on a Thermo-Finnigan Trace DSQ fast-scanning

single-quadrupole MS operated at unit mass resolving power with electron impact ionization and a 50–750 atomic mass unit scan range. The instrument is tuned and calibrated for mass resolution and mass accuracy daily.

Compound Identification, Quantification, and Data Curation: Metabolites were identified by automated comparison of the ion features in the experimental samples to a reference library of chemical standard entries that included retention time, molecular weight (m/z), preferred adducts, and in-source fragments as well as associated MS spectra and curated by visual inspection for quality control using software developed at Metabolon [37]. Identification of known chemical entities was based on comparison to metabolomic library entries of more than 2,800 commercially-available purified standards. Subsequent QC and curation processes were utilized to ensure accurate, consistent identification and to minimize system artifacts, mis-assignments, and background noise. Library matches for each compound were verified for each sample. Peaks were quantified using area under the curve. Raw area counts for each metabolite in each sample were normalized to correct for variation resulting from instrument inter-day tuning differences by the median value for each run-day, therefore setting the medians to 1.0 for each run. This preserved variation between samples but allowed metabolites of widely different raw peak areas to be compared on a similar graphical scale. Missing values were imputed with the observed minimum after normalization. The present dataset comprises a total of 571 compounds of known identity (named biochemicals).

Bioinformatics: The LIMS system encompasses sample accessioning, preparation, instrument analysis and reporting, and advanced data analysis. Additional informatics components include data extraction into a relational database and peak-identification software; proprietary data processing tools for QC and compound identification; and a collection of interpretation and visualization tools for use by data analysts. The hardware and software systems are built on a web-service platform utilizing Microsoft's.NET technologies which run on high-performance application servers and fiber-channel storage arrays in clusters to provide active failover and load-balancing.

Statistical Analysis

All statistical analyses were completed using GraphPad Prism 7 (GraphPad, San Diego, CA, USA). Two-way ANOVA was performed for determination of differences between groups followed by Tukey's multiple comparisons test. Levels of statistical significance were reached when $p < 0.05$. For Metabolon, missing values in the data are assumed to be below the level of detection of the used instruments. Log transformations and imputation of missing values with the minimum observed values for each metabolite was conducted. This was followed by the usage of ANOVA to identify biochemicals that were significantly different between groups. Given the multiple comparisons inherent in analysis of metabolites, between-group relative differences are assessed using both p-value and false discovery rate analysis (q-value).

Results

I. Rapamycin enhances Aβ clearance in the E4FAD mice

We found that rapamycin restored BBB function in the E4FAD mice (E4FAD-Rapa). Figure 1A shows the representative confocal images of capillaries; the intensity of fluorescence in the capillary lumen reflects the amount of P-gp, an efflux transporter of Aβ. The corresponding quantitative results are shown in Figure 1B; the E4FAD-Control mice had significantly reduced P-gp transport activity ($p < 0.001$) compared to the E3FAD-Control mice. Rapamycin did not have significant effects for E3FAD mice, but did for the E4FAD mice; E4FAD-Rapa group had restored P-gp activity to the level similar to that of the E3FAD-Rapa group (Fig. 1B). The finding was confirmed by the P-gp protein expression levels determination using Western blotting (Fig. 1C). The findings from P-gp were consistent with the Aβ immunochemistry staining — Rapamycin significantly reduce Aβ retention in the E4FAD mice but did not have significance effects in the E3FAD mice (Figs. 2A and 2B). Collectively, our results show that rapamycin was able to enhance BBB function for Aβ clearance and reduce Aβ retention in the asymptomatic E4FAD mice.

II. Rapamycin restores cerebral blood flow (CBF) in the E4FAD female mice

We observed reduced global CBF in the E4FAD-Control mice at 2 months of age compared with the age-matched E3FAD mice (Fig. 3A). The CBF level is colorized in a linear scale. After 16 weeks of feeding, we found that rapamycin restored hippocampal CBF of the E4FAD mice to the level similar to those in the E3FAD-Control and E3FAD-Rapa mice (Fig. 3B). Whether treated rapamycin or not, E3FAD mice did not show significantly differences in hippocampal CBF. We further calculated the CBF percent changes between post- and pre-treatment in each group (Fig. 3C). We found that, E4FAD-Rapa mice showed significant improvement in CBF, which was not observed in both of the E3FAD groups and the E4FAD-Control group. We further stratified with sex and found that rapamycin had particularly significant effects in E4FAD female mice (Fig. 3D). Taken together, we showed that rapamycin was effective to restore CBF in the E4FAD mice, especially in the females.

III. Rapamycin preserves neurotransmitters and neuronal integrity in the E4FAD mice

The *in vivo* brain metabolites were determined using ^{1}H-MRS. Figure 4A shows the voxel replacement on bilateral hippocampus for MRS experiments. Figure 4B demonstrates a representative spectrum of ^{1}H-MRS, showing peaks of lactate (Lac), N-acetyl-aspartate (NAA), glutamate (Glu) and glutamine (Gln), creatine (Cr), glycerophosphocholine (GPC) and phosphocholine (PCh), taurine (Tau) and myo-inositol (mI). We found that with 16 weeks of rapamycin intervention, E4FAD mice (E4FAD-Rapa) had increases in GPC/PCh (Fig. 4C), Glu/Gln (Fig. 4D) and NAA (Fig. 4E). In contrast, E4FAD-Control mice showed decreases in these metabolites during the 16 weeks of period (between 3 and 7 months of age). Therefore, there shows a significant difference in changes of the metabolites between the E4FAD-Control and E4FAD-Rapa group ($p < 0.01$). This difference was not seen in the E3FAD mice. GPC and PCh have been shown to increases the release of the neurotransmitter acetylcholine and facilitates learning and memory [38]; Glu and Gln are excitatory neurotransmitters; and NAA has been used as indicator of neuronal health as it is

most abundant in neurons [39]. Therefore, our results suggest that rapamycin is able to preserve neurotransmitter levels and neuronal integrity of the E4FAD mice.

IV. Rapamycin induces different brain metabolic changes in E3FAD and E4FAD mice

Among 571 identified biochemicals through metabolomics analysis, 36 and 73 metabolites showed significant changes between Rapamycin and Control mice in the APOE4 and APOE3 group, respectively (Supplement Table 1 and Table 2). Notably, rapamycin decreased free fatty acids (FFA) levels in the E4FAD mice. Table 3 shows the fold change (FC) of each metabolite by comparison the level at Rapamycin vs. Control in each genotype. Compared with E4FAD-Control, E4FAD-Rapa mice had significantly reduced FFA that involves several long-chain fatty acids and polyunsaturated fatty acid. There was no change in FFA between the E3FAD-Control and E3FAD-Rapa mice (Table 3). On the other hand, we observed that E3FAD-Rapa mice had a reduced level in many intermediate metabolites associated with glycolysis and the tricarboxylic acid (TCA) cycle. We found that three glycolytic intermediates (pyruvate, lactate and glycerate) and two TCA cycle intermediates (fumarate and malate) are significantly lower ($p < 0.05$) in the E3FAD-Rapa group compared to controls. Decreases in TCA intermediates are generally ascribed to lower input of glucose derived acetyl-CoA (from glycolysis), if without a concomitant increase in lipid β-oxidation. To confirm that, we examined a marker of β-oxidation, the ketone body 3-hydroxybutyrate, and it was also lower in the E3FAD-Rapa brains compared to controls. Table 4 shows the FC of each metabolite by comparison the level at Rapamycin vs. Control in each genotype. We found that E3FAD-Rapa mice also had other glycolysis and carbohydrate pathways that are altered by rapamycin. Specifically, biochemicals in the pentose phosphate pathway (PPP), the fructose/mannose/galactose metabolism, the nucleotide sugars, and amino sugars. The decreased levels of glycolytic intermediates are consistent with a slowdown in overall carbohydrate metabolism and utilization. Concomitant decreases in PPP and other carbohydrate pathways are common when glucose uptake or utilization becomes lower. Taken together, it shows that rapamycin induced different metabolic effects in the E3FAD and E4FAD mice; E4FAD appears to normalize lipid-associated metabolism, whereas E3FAD mice appears to slow overall glucose-associated metabolism. For comparison purpose, the quantitative values of each aforementioned metabolite in each group can be found in Supplement Table 3.

V. Rapamycin enhances white matter structural integrity in E3FAD and E4FAD mice

White matter microstructural integrity was determined by DTI measures of fractional anisotropy (FA) and mean diffusivity (MD). Figure 5A shows the images of FA, MD, and diffusion-encoded-color (DEC) maps of the four groups of mice. FA, the degree to which water diffuses in one direction (along the axon), is the most common measure used to assess axonal integrity. MD is a measure of the degree of restriction to diffusion of water molecules, irrespective of direction. high values of FA suggest more highly organized, strongly myelinated tracts. Whereas low values for MD are consistent with greater organization of brain structure [40]. Figure 5B shows the quantitative FA values, which did not differ between E3FAD-Control and E3FAD-Rapa group. The FA values had a trending of increases in corpus collasum, cortex, hippocampus, and reaching to significance in thalamus (0.26±0.04/0.35±0.08, p<0.03), in the E4FAD-Rapa mice compared to the E4FAD-

Controls. This suggests that rapamycin protects white matter axons in the E4FAD mice. On the other hand, MD values were significantly lower across cortical and subcortical regions in both E3FAD-Rapa and E4FAD-Rapa groups compared to controls, indicating higher cellularity or improvements in microstructural integrity induced by rapamycin for both E3FAD and E4FAD mice (Fig. 5C).

VI. Rapamycin increases brain water content in E3FAD and E4FAD mice

Figure 6A shows the maps of water content in the brain (indexed by BBPC) and Figure 6B shows the corresponding quantitative values. Rapamycin increased water content; we found that BBPC significantly increased in both E3FAD-Rapa and E4FAD-Rapa mice.

VII. Rapamycin induces different hindpaw stimulation and cerebrovascular reactivity responses in E3FAD and E4FAD mice

We did not find significant BOLD signal changes in the ipsilateral somatosensory (S1FL) region during unilateral hindpaw stimulation (Fig. 7A). BOLD response magnitudes across control and rapamycin diet during hindpaw stimulations are not statistically significant in either E3FAD or E4FAD group. Figure 7B shows the statistical maps of CVR from the hypercapnia experiments in the E4FAD mice (Left: Control group; Right: Rapamycin group). The color code shows the percent BOLD change in the linear scale. Rapamycin did not alter overall CVR responses in E4FAD mice, however, when did regional analysis, we found that E4FAD- Rapa group showed a significantly larger effect in hippocampus (Fig. 7B; bottom right). In contrast, E3FAD-Rapa mice show overall lower in the magnitude, time to peak in BOLD response compared to the E3FAD-Control (Fig. 7C; bottom left). The differences in magnitude and shape of BOLD response across other regions including somatosensory, thalamic, and hippocampal regions (Fig. 7C; bottom right).

VIII. Rapamycin differentially enhances memory and reduces anxiety in the EFAD mice

E3FAD-Cotnrol and E4-Cotnrol mice did not show differences in the NOR test, indicating that E4FAD mice still had similar cognitive capacity at the 7–8 months of age compared to the E3FAD mice (Fig. 8A). Interestingly, we found the both E3FAD-Rapa and E4FAD-Rapa mice both had higher D_2 index compared to their controls, suggesting rapamycin enhanced recognition memory independent of APOE genotype (Fig. 8A). When looking at anxiety level assessed by EPM, we did not find significant differences between the E4FAD-Control and E4FAD-Rapa mice, although rapamycin treatment group had a trend of spending more time in open arms. In contrast, E3FAD-Rapa mice spent significantly longer time in the open arms compared to the control group ($p<0.01$; Fig. 8B), indicating lower anxiety level with rapamycin treatment.

Discussion

In this study, we demonstrated that rapamycin was able to restore vascular and metabolic functions in the young adult mice that carried human APOE4 gene, and there were pharmacogenetic effects in response to rapamycin between the E3FAD and E4FAD mice. For the E4FAD mice, rapamycin normalized bodyweight, restored CBF, BBB activity for Aβ transport, neurotransmitter levels, neuronal integrity and FFA level, and reduced Aβ

retention, compared to their APOE3 littermates (Table 5). Both male and female mice were subjects to the experiments, however, only in the CBF measurements did we see a sex difference. Rapamycin did not show effects in these measures for the E3FAD mice. Furthermore, E3FAD-Rapa mice had lower CVR responses, lower anxiety and reduced glycolysis in the brain, which were not seen in the E4FAD-Rapa mice. On the other hand, rapamycin enhanced overall water content, water diffusion (cellularity) in white matter, and spatial memory in both E3FAD and E4FAD mice, but did not impact the somatosensory responses under hindpaw stimulation (Table 5).

Our findings are consistent with the literature that APOE4 carriers had reduced CBF and accumulated Aβ long before cognitive impairment appears (e.g., at 2 months of age) [41]. We showed that rapamycin was able to restore CBF and BBB integrity, and further enhanced spatial memory in the asymptomatic E4FAD mice, similar to what we found previously using another APOE4 transgenic mouse model [16]. Restoration of CBF by rapamycin observed in the present study was also in agreement with another study in symptomatic mice that modeled human AD ((h)APP mice) [42]. The mechanism of action may involve in inhibition of the mechanistic target of rapamycin (mTOR) signaling and activation of endothelial nitric oxide synthase (eNOS) pathways as suggested previously [16, 42]. In the present study, we further demonstrated that rapamycin was more effective in restoring CBF for the E4FAD female mice, which is consistent with other studies showing that rapamycin benefits females more than males, including greater effects on lifespan [43–45]. One possibility for this is sex-specific differences in rapamycin uptake for metabolism, where female mice have higher blood levels of rapamycin than males when equal concentration of rapamycin was provided in the diet [46]. Furthermore, CBF is tightly coupled with brain energy demand for neurotransmission, known as vascular-metabolism coupling [47–49]. This is consistent with our results from ^{1}H-MRS in which E4FAD-Rapa mice had preserved neurotransmitter levels compared to the E4FAD-Control mice.

We previously reported that rapamycin prevents BBB leakage in an APOE4 transgenic mice, which may be due to suppressing inflammation through the cyclophilin A- related proinflammatory pathways [16, 50]. In the current study, we further demonstrated that rapamycin was able to restore quantity and activity of the P-gp transporter, which is an ATP-driven transporter highly expressed at the BBB that facilitates clearance of Aβ. The underlying mechanism is currently unclear, which will need to be identified in the future studies.

The vulnerability of APOE4 carriers is correlated with variance in lipid metabolism as a result of the apoE lipid transport protein structural variance, where ApoE4 proteins have a binding preference for large triglyceride-rich very-low-density lipoprotein (VLDL), forming neurotoxic complexes [51]. It has been previously shown that mTOR inhibition by rapamycin is able to modulate lipid metabolism and prevent oxidative stress and triglyceride accumulation, and provide less triglyceride-rich VLDL for apoE4 to interact [52]. It is consistent with our funding that rapamycin was able to normalize long-chain and polyunsaturated fatty acids in E4FAD mice that are related to inflammation and VLDL interactions within E4 genotypes. Reducing the level of inflammation could further prevent

Aβ aggregation. Normalization of lipid levels might also explain the bodyweight normalization see in the E4FAD-Rapa mice.

ApoE3 proteins, on the other hand, has a preference for binding with small phospholipid rich high-density lipoprotein, and thus leads to lower neuroinflammation and a relatively heathier status compared to ApoE4. It may explain why we did not see the vascular and metabolic deficits in the E3FAD-Control compared to the E4FAD-Control mice, and why rapamycin did not have much effect on the E3FAD mice. Instead of normalizing lipid profile, rapamycin exerted effects on glycolytic pathways of the E3FAD mice. The phenomenon observed in the E3FAD –Rapa mice is similar to what has been observed in the caloric restriction (CR) condition; Inhibition of mTOR in relatively healthy animals has been shown to reduce glucose uptake and extend longevity [53, 54]. While rapamycin extension of longevity for the E3FAD mice remains to be investigated, the lower anxiety and enhanced memory found in the E3FAD-Rapa mice was consistent with what have been observed in the previous studies [23, 55]. Supported by literature, it has been shown that mTOR is able to target different pathways, including lipid metabolism via SREBP1/PPARγ and glycolysis via HIF1α pathways [56]. We hypothesize that rapamycin might target more on the SREBP1/PPARγ pathways in the E4FAD mice, while more on the HIF1α pathways in the E3FAD mice. Thus, the pharmacogenetic effects between E3FAD and E4FAD may result from the different signaling pathways that rapamycin exerted in coordinating with the physiological environment induced by different APOE genotype. Future studies will be needed to verify the hypothesis.

An interesting aspect we found in the study is that rapamycin enhanced overall water content and water diffusion in white matter (lower MD values) in both E3FAD and E4FAD mice (Table 5). This finding suggests that rapamycin might be able to preserve water homeostasis in the brain and thus protect cellular integrity of the white matter. As the mammalian central nervous system (CNS) is separated from the blood by tight junctions, collectively termed BBB, this imposes unique features of solvent and water movement into and out of the CNS [57]. The preservation of BBB in the E4FAD mice might help the water content enhancement. On the other hand, changes in glucose level in the E3FAD mice might also impact the osmosis. Lower glucose levels also result in more water being reabsorbed by the kidneys, causing higher amounts of water to be retained in the body and increasing hydration [58]. As brain dehydration is associated with cognitive impairment [26], our results are in line with literature that increasing in brain water content is associated with enhanced memory as observed in the E3FAD and E4FAD mice. Interestingly, rapamycin seems to affect the cognitive more than the non-cognitive component (e.g., the somatosensory function); we did not see significant effects under hindpaw stimulation in either E3FAD-Rapa or E4FAD-Rapa mice.

In this study, using the multimodal MRI methods and biochemical assays, we showed that rapamycin is beneficial to both E3FAD and E4FAD mice. Rapamycin is particularly effective in prevention of AD for young E4FAD mice by restoring brain vascular and metabolic functions, and inhibiting Aβ retention. Rapamycin is shown to enhance many functionalities of the E3FAD mice, similar to the effects of CR. Our results indicate an APOE-dependent pharmacogenetic response to rapamycin for preventing AD. As the MRI

methods used in the study are all available and approved for human use (e.g., ASL, ^{1}H-MRS, DTI and fMRI) and rapamycin is FDA-approved, our findings may have immediate translational value for clinical investigation [59]. As young, cognitively normal APOE4 carriers develop brain vascular and metabolic deficits decades before showing AD symptoms, early detection of brain physiological changes and intervention with effective therapeutics would be critical for APOE4 carriers to prevent AD [15]. Non-invasive MRI methods will allow early diagnosis and longitudinal follow-up for treatment efficacy as well as allowing researchers to assess appropriate timing to administer rapamycin to individuals based on observed neurophysiological changes. Further investigation will also be needed to identify APOE-dependent pharmacogenetic responses to rapamycin in humans, and to quantify the risks of prolonged use of rapamycin.

A limitation of the study is that the mouse model does not produce NFT, therefore, we were not able to identify the role of tau in the present study. Future studies will be needed to identify rapamycin effectiveness in an APOE mouse model with NFT. Future studies will also be needed to identify the mechanism that drives the pharmacogenetic responses to rapamycin between the APOE3 and APOE4 genotypes. In particular, it would be important to determine if the pathways (e.g., lipid metabolism vs. glycolysis) that mTOR signaling to are APOE genotype-dependent.

In conclusion, we showed that rapamycin was able to restore brain functions and reduce AD risk for young, asymptomatic mice that were with human APOE4 gene. We also demonstrated that E3FAD mice responded differently to rapamycin compared to the E4FAD mice, indicating a pharmacogenetic difference to rapamycin depending on the APOE genotypes. As the multi-modal MRI methods used in the study are readily to be used in humans and rapamycin is FDA-approved, our results may pave a way for future clinical testing of the pharmacogenetic responses in humans with different APOE alleles, and potentially using rapamycin to prevent AD for asymptomatic APOE4 carriers.

Supplementary Material

Refer to Web version on PubMed Central for supplementary material.

Acknowledgments

Funding.

The work was supported by funding from the National Institutes of Health (NIH) (R01AG054459 and RF1AG062480 to A-LL), NIH CTSA at the University of Kentucky (UL1TR0000117; pilot grant to A-LL), Donors Cure Foundation (to A-LL), and NIH Training Grant (T32DK007778 to LMY). The 7T ClinScan small animal MRI scanner of the UK was funded by the S10 NIH Shared Instrumentation Program Grant (1S10RR029541-01). The content is solely the responsibility of the authors and does not necessarily represent the official views of the National Institute on Aging or the National Institutes of Health. SDM is employed by Metabolon Inc.. Metabolon Inc. provided support in the form of salary for author SDM but did not have any additional role in the study design, data collection and analysis, decision to publish, or preparation of the manuscript.

References

1. Shaw LM, Vanderstichele H, Knapik-Czajka M, Clark CM, Aisen PS, Petersen RC, et al. Cerebrospinal fluid biomarker signature in Alzheimer's disease neuroimaging initiative subjects. Annals of Neurology. 2009;65(4):403–13. doi: 10.1002/ana.21610. [PubMed: 19296504]
2. Janocko NJ, Brodersen KA, Soto-Ortolaza AI, Ross OA, Liesinger AM, Duara R, et al. Neuropathologically defined subtypes of Alzheimer's disease differ significantly from neurofibrillary tangle-predominant dementia. Acta Neuropathologica. 2012;124(5):681–92. doi: 10.1007/s00401-012-1044-y. [PubMed: 22968369]
3. Fleisher AS, Chen K, Liu X, Ayutyanont N, Roontiva A, Thiyyagura P, et al. Apolipoprotein E epsilon4 and age effects on florbetapir positron emission tomography in healthy aging and Alzheimer disease. Neurobiol Aging. 2013;34(1):1–12. Epub 2012/05/29. doi: 10.1016/j.neurobiolaging.2012.04.017. [PubMed: 22633529]
4. Farrer LA, Cupples LA, Haines JL, Hyman B, Kukull WA, Mayeux R, et al. Effects of age, sex, and ethnicity on the association between apolipoprotein E genotype and Alzheimer disease. A meta-analysis. APOE and Alzheimer Disease Meta Analysis Consortium. Jama. 1997;278(16):1349–56. Epub 1997/10/29. [PubMed: 9343467]
5. Raber J, Huang Y, Ashford JW. ApoE genotype accounts for the vast majority of AD risk and AD pathology. Neurobiol Aging. 2004;25(5):641–50. Epub 2004/06/03. doi: 10.1016/j.neurobiolaging.2003.12.023. [PubMed: 15172743]
6. Thambisetty M, Beason-Held L, An Y, Kraut MA, Resnick SM. APOE epsilon4 genotype and longitudinal changes in cerebral blood flow in normal aging. Archives of neurology. 2010;67(1):93–8. Epub 2010/01/13. doi: 10.1001/archneurol.2009.913. [PubMed: 20065135]
7. Reiman EM, Chen K, Alexander GE, Caselli RJ, Bandy D, Osborne D, et al. Correlations between apolipoprotein E epsilon4 gene dose and brain-imaging measurements of regional hypometabolism. Proceedings of the National Academy of Sciences of the United States of America. 2005;102(23):8299–302. Epub 2005/06/04. doi: 10.1073/pnas.0500579102. [PubMed: 15932949]
8. Reiman EM, Caselli RJ, Chen K, Alexander GE, Bandy D, Frost J. Declining brain activity in cognitively normal apolipoprotein E epsilon 4 heterozygotes: A foundation for using positron emission tomography to efficiently test treatments to prevent Alzheimer's disease. Proceedings of the National Academy of Sciences of the United States of America. 2001;98(6):3334–9. doi: 10.1073/pnas.061509598. [PubMed: 11248079]
9. Reiman EM, Chen K, Alexander GE, Caselli RJ, Bandy D, Osborne D, et al. Functional brain abnormalities in young adults at genetic risk for late-onset Alzheimer's dementia. Proceedings of the National Academy of Sciences of the United States of America. 2004;101(1):284–9. Epub 2003/12/23. doi: 10.1073/pnas.2635903100. [PubMed: 14688411]
10. Hays CC, Zlatar ZZ, Meloy MJ, Bondi MW, Gilbert PE, Liu TT, et al. APOE modifies the interaction of entorhinal cerebral blood flow and cortical thickness on memory function in cognitively normal older adults. Neuroimage. 2019;202:116162. doi: 10.1016/j.neuroimage.2019.116162. [PubMed: 31493534]
11. Bangen KJ, Beiser A, Delano-Wood L, Nation DA, Lamar M, Libon DJ, et al. APOE genotype modifies the relationship between midlife vascular risk factors and later cognitive decline. J Stroke Cerebrovasc Dis. 2013;22(8):1361–9. doi: 10.1016/j.jstrokecerebrovasdis.2013.03.013. [PubMed: 23601373]
12. Nierenberg J, Pomara N, Hoptman MJ, Sidtis JJ, Ardekani BA, Lim KO. Abnormal white matter integrity in healthy apolipoprotein E epsilon4 carriers. Neuroreport. 2005;16(12):1369–72. [PubMed: 16056141]
13. Persson J, Lind J, Larsson A, Ingvar M, Cruts M, Van Broeckhoven C, et al. Altered brain white matter integrity in healthy carriers of the APOE ε4 allele. Neurology. 2006;66(7):1029. doi: 10.1212/01.wnl.0000204180.25361.48. [PubMed: 16606914]
14. Mormino EC, Betensky RA, Hedden T, Schultz AP, Ward A, Huijbers W, et al. Amyloid and APOE epsilon4 interact to influence short-term decline in preclinical Alzheimer disease. Neurology. 2014;82(20):1760–7. Epub 2014/04/22. doi: 10.1212/WNL.0000000000000431. [PubMed: 24748674]

15. Lin AL, Butterfield DA, Richardson A. mTOR: Alzheimer's disease prevention for APOE4 carriers. Oncotarget. 2016;7(29):44873–4. Epub 2016/07/08. doi: 10.18632/oncotarget.10349. [PubMed: 27385004]

16. Lin AL, Jahrling JB, Zhang W, DeRosa N, Bakshi V, Romero P, et al. Rapamycin rescues vascular, metabolic and learning deficits in apolipoprotein E4 transgenic mice with pre-symptomatic Alzheimer's disease. J Cereb Blood Flow Metab. 2017;37(1):217–26. Epub 2016/01/02. doi: 10.1177/0271678X15621575. [PubMed: 26721390]

17. Oddo S The role of mTOR signaling in Alzheimer disease. Front Biosci (Schol Ed). 2012;4:941–52. Epub 2011/12/29. doi: 10.2741/s310. [PubMed: 22202101]

18. Pei JJ, Hugon J. mTOR-dependent signalling in Alzheimer's disease. J Cell Mol Med. 2008;12(6B):2525–32. Epub 2009/02/13. doi: 10.1111/j.1582-4934.2008.00509.x. [PubMed: 19210753]

19. Majumder S, Richardson A, Strong R, Oddo S. Inducing autophagy by rapamycin before, but not after, the formation of plaques and tangles ameliorates cognitive deficits. PLoS One. 2011;6(9):e25416 Epub 2011/10/08. doi: 10.1371/journal.pone.0025416. [PubMed: 21980451]

20. Spilman P, Podlutskaya N, Hart MJ, Debnath J, Gorostiza O, Bredesen D, et al. Inhibition of mTOR by rapamycin abolishes cognitive deficits and reduces amyloid-beta levels in a mouse model of Alzheimer's disease. PLoS One. 2010;5(4):e9979 Epub 2010/04/09. doi: 10.1371/journal.pone.0009979. [PubMed: 20376313]

21. Tai LM, Balu D, Avila-Munoz E, Abdullah L, Thomas R, Collins N, et al. EFAD transgenic mice as a human APOE relevant preclinical model of Alzheimer's disease. J Lipid Res. 2017;58(9):1733–55. Epub 2017/04/09. doi: 10.1194/jlr.R076315. [PubMed: 28389477]

22. Youmans KL, Tai LM, Nwabuisi-Heath E, Jungbauer L, Kanekiyo T, Gan M, et al. APOE4-specific changes in Abeta accumulation in a new transgenic mouse model of Alzheimer disease. The Journal of biological chemistry. 2012;287(50):41774–86. Epub 2012/10/13. doi: 10.1074/jbc.M112.407957. [PubMed: 23060451]

23. Parikh I, Guo J, Chuang KH, Zhong Y, Rempe RG, Hoffman JD, et al. Caloric restriction preserves memory and reduces anxiety of aging mice with early enhancement of neurovascular functions. Aging (Albany NY). 2016;8(11):2814–26. doi: 10.18632/aging.101094. [PubMed: 27829242]

24. Guo J, Bakshi V, Lin AL. Early Shifts of Brain Metabolism by Caloric Restriction Preserve White Matter Integrity and Long-Term Memory in Aging Mice. Front Aging Neurosci. 2015;7:213 Epub 2015/12/01. doi: 10.3389/fnagi.2015.00213. [PubMed: 26617514]

25. Hoffman JD, Yanckello LM, Chlipala G, Hammond TC, McCulloch SD, Parikh I, et al. Dietary inulin alters the gut microbiome, enhances systemic metabolism and reduces neuroinflammation in an APOE4 mouse model. PLoS One. 2019;14(8):e0221828 Epub 2019/08/29. doi: 10.1371/journal.pone.0221828. [PubMed: 31461505]

26. Lauriola M, Mangiacotti A, D'Onofrio G, Cascavilla L, Paris F, Paroni G, et al. Neurocognitive Disorders and Dehydration in Older Patients: Clinical Experience Supports the Hydromolecular Hypothesis of Dementia. Nutrients. 2018;10(5). doi: 10.3390/nu10050562.

27. Thalman SW, Powell DK, Lin A-L. Novel Calibrated Short TR Recovery (CaSTRR) Method for Brain-Blood Partition Coefficient Correction Enhances Gray-White Matter Contrast in Blood Flow Measurements in Mice. Front Neurosci. 2019;13:308–. doi: 10.3389/fnins.2019.00308. [PubMed: 31001077]

28. Thalman SW, Powell DK, Ubele M, Norris CM, Head E, Lin AL. Brain-Blood Partition Coefficient and Cerebral Blood Flow in Canines Using Calibrated Short TR Recovery (CaSTRR) Correction Method. Front Neurosci. 2019;13:1189. doi: 10.3389/fnins.2019.01189. [PubMed: 31749679]

29. Leithner C, Müller S, Füchtemeier M, Lindauer U, Dirnagl U, Royl G. Determination of the Brain–Blood Partition Coefficient for Water in Mice Using MRI. Journal of Cerebral Blood Flow & Metabolism. 2010;30(11):1821–4. doi: 10.1038/jcbfm.2010.160.. [PubMed: 20842161]

30. Lin AL, Pulliam DA, Deepa SS, Halloran JJ, Hussong SA, Burbank RR, et al. Decreased in vitro mitochondrial function is associated with enhanced brain metabolism, blood flow, and memory in Surf1-deficient mice. J Cereb Blood Flow Metab. 2013;33(10):1605–11. Epub 2013/07/11. doi: 10.1038/jcbfm.2013.116. [PubMed: 23838831]

31. Bachstetter AD, Webster SJ, Tu T, Goulding DS, Haiech J, Watterson DM, et al. Generation and behavior characterization of CaMKIIbeta knockout mice. PLoS One. 2014;9(8):e105191 Epub 2014/08/16. doi: 10.1371/journal.pone.0105191. [PubMed: 25127391]
32. Hoffman JD, Parikh I, Green SJ, Chlipala G, Mohney RP, Keaton M, et al. Age Drives Distortion of Brain Metabolic, Vascular and Cognitive Functions, and the Gut Microbiome. Front Aging Neurosci. 2017;9:298. doi: 10.3389/fnagi.2017.00298. [PubMed: 28993728]
33. Ma D, Wang A, Parikh I, Green SJ, Hoffman JD, Chlipala G, et al. Ketogenic diet enhances neurovascular function with altered gut microbiome in young healthy mice. Scientific Reports. 2018; 8:6670. doi: 10.1038/s41598-018-25190-5. [PubMed: 29703936]
34. Yanckello LM, Young LEA, Hoffman JD, Mohney RP, Keaton MA, Abner E, et al. Caloric Restriction Alters Postprandial Responses of Essential Brain Metabolites in Young Adult Mice. Front Nutr. 2019;6:90. doi: 10.3389/fnut.2019.00090. [PubMed: 31249833]
35. Evans AM, Bridgewater BR, Liu Q, Mitchell MW, Robinson RJ, Dai H, et al. High Resolution Mass Spectrometry Improves Data Quantity and Quality as Compared to Unit Mass Resolution Mass Spectrometry in High- Throughput Profiling Metabolomics. Metabolomics. 2014;4(132).
36. Ohta T, Masutomi N, Tsutsui N, Sakairi T, Mitchell M, Milburn MV, et al. Untargeted metabolomic profiling as an evaluative tool of fenofibrate-induced toxicology in Fischer 344 male rats. Toxicologic pathology. 2009;37(4):521–35. Epub 2009/05/22. doi: 10.1177/0192623309336152. [PubMed: 19458390]
37. Dehaven CD, Evans AM, Dai H, Lawton KA. Organization of GC/MS and LC/MS metabolomics data into chemical libraries. J Cheminform. 2010;2(1):9. doi: 10.1186/1758-2946-2-9. [PubMed: 20955607]
38. Bahous RH, Jadavji NM, Deng L, Cosin-Tomas M, Lu J, Malysheva O, et al. High dietary folate in pregnant mice leads to pseudo-MTHFR deficiency and altered methyl metabolism, with embryonic growth delay and short-term memory impairment in offspring. Hum Mol Genet. 2017;26(5):888–900. doi: 10.1093/hmg/ddx004. [PubMed: 28069796]
39. Schuff N, Meyerhoff DJ, Mueller S, Chao L, Sacrey DT, Laxer K, et al. N-acetylaspartate as a marker of neuronal injury in neurodegenerative disease. Adv Exp Med Biol. 2006;576:241–62; discussion 361–3. doi: 10.1007/0-387-30172-0_17. [PubMed: 16802717]
40. Clark KA, Nuechterlein KH, Asarnow RF, Hamilton LS, Phillips OR, Hageman NS, et al. Mean diffusivity and fractional anisotropy as indicators of disease and genetic liability to schizophrenia. J Psychiatr Res. 2011;45(7):980–8. Epub 2011/02/11. doi: 10.1016/j.jpsychires.2011.01.006. [PubMed: 21306734]
41. Hays CC, Zlatar ZZ, Wierenga CE. The Utility of Cerebral Blood Flow as a Biomarker of Preclinical Alzheimer's Disease. Cell Mol Neurobiol. 2016;36(2):167–79. doi: 10.1007/s10571-015-0261-z. [PubMed: 26898552]
42. Lin AL, Zheng W, Halloran JJ, Burbank RR, Hussong SA, Hart MJ, et al. Chronic rapamycin restores brain vascular integrity and function through NO synthase activation and improves memory in symptomatic mice modeling Alzheimer's disease. J Cereb Blood Flow Metab. 2013;33(9):1412–21. Epub 2013/06/27. doi: 10.1038/jcbfm.2013.82. [PubMed: 23801246]
43. Arriola Apelo SI, Lamming DW. Rapamycin: An InhibiTOR of Aging Emerges From the Soil of Easter Island. J Gerontol A Biol Sci Med Sci. 2016;71(7):841–9. Epub 2016/05/21. doi: 10.1093/gerona/glw090. [PubMed: 27208895]
44. Harrison DE, Strong R, Sharp ZD, Nelson JF, Astle CM, Flurkey K, et al. Rapamycin fed late in life extends lifespan in genetically heterogeneous mice. Nature. 2009;460(7253):392–5. Epub 2009/07/10. doi: 10.1038/nature08221. [PubMed: 19587680]
45. Pan Z, Chang C. Gender and the regulation of longevity: implications for autoimmunity. Autoimmun Rev. 2012;11(6–7):A393–403. Epub 2011/12/21. doi: 10.1016/j.autrev.2011.12.004. [PubMed: 22182796]
46. Miller RA, Harrison DE, Astle CM, Fernandez E, Flurkey K, Han M, et al. Rapamycin-mediated lifespan increase in mice is dose and sex dependent and metabolically distinct from dietary restriction. Aging Cell. 2014;13(3):468–77. doi: 10.1111/acel.12194. [PubMed: 24341993]

47. Fox PT, Raichle ME. Focal physiological uncoupling of cerebral blood flow and oxidative metabolism during somatosensory stimulation in human subjects. Proc Natl Acad Sci U S A. 1986;83(4):1140–4. doi: 10.1073/pnas.83.4.1140. [PubMed: 3485282]

48. Fox PT, Raichle ME, Mintun MA, Dence C. Nonoxidative glucose consumption during focal physiologic neural activity. Science. 1988;241(4864):462–4. [PubMed: 3260686]

49. Lin AL, Fox PT, Hardies J, Duong TQ, Gao JH. Nonlinear coupling between cerebral blood flow, oxygen consumption, and ATP production in human visual cortex. Proc Natl Acad Sci U S A. 2010;107(18):8446–51. doi: 10.1073/pnas.0909711107. [PubMed: 20404151]

50. Bell RD, Winkler EA, Singh I, Sagare AP, Deane R, Wu Z, et al. Apolipoprotein E controls cerebrovascular integrity via cyclophilin A. Nature. 2012;485(7399):512–6. Epub 2012/05/25. doi: 10.1038/nature11087. [PubMed: 22622580]

51. Huang Y, Mahley RW. Apolipoprotein E: structure and function in lipid metabolism, neurobiology, and Alzheimer's diseases. Neurobiol Dis. 2014;72 Pt A:3–12. Epub 2014/08/27. doi: 10.1016/j.nbd.2014.08.025. [PubMed: 25173806]

52. Caron A, Richard D, Laplante M. The Roles of mTOR Complexes in Lipid Metabolism. Annual Review of Nutrition. 2015;35(1):321–48. doi: 10.1146/annurev-nutr-071714-034355.

53. Lee J, Yanckello LM, Ma D, Hoffman JD, Parikh I, Thalman S, et al. Neuroimaging Biomarkers of mTOR Inhibition on Vascular and Metabolic Functions in Aging Brain and Alzheimer's Disease. Front Aging Neurosci. 2018;10:225. doi: 10.3389/fnagi.2018.00225. [PubMed: 30140223]

54. Perluigi M, Di Domenico F, Butterfield DA. mTOR signaling in aging and neurodegeneration: At the crossroad between metabolism dysfunction and impairment of autophagy. Neurobiol Dis. 2015;84:39–49. doi: 10.1016/j.nbd.2015.03.014. [PubMed: 25796566]

55. Halloran J, Hussong SA, Burbank R, Podlutskaya N, Fischer KE, Sloane LB, et al. Chronic inhibition of mammalian target of rapamycin by rapamycin modulates cognitive and non-cognitive components of behavior throughout lifespan in mice. Neuroscience. 2012;223:102–13. Epub 2012/07/04. doi: 10.1016/j.neuroscience.2012.06.054. [PubMed: 22750207]

56. Mao Z, Zhang W. Role of mTOR in Glucose and Lipid Metabolism. Int J Mol Sci. 2018;19(7). doi: 10.3390/ijms19072043.

57. Kimelberg HK. Water homeostasis in the brain: basic concepts. Neuroscience. 2004;129(4):851–60. doi: 10.1016/j.neuroscience.2004.07.033. [PubMed: 15561403]

58. Ainslie PN, Campbell IT, Frayn KN, Humphreys SM, MacLaren DP, Reilly T, et al. Energy balance, metabolism, hydration, and performance during strenuous hill walking: the effect of age. J Appl Physiol (1985). 2002;93(2):714–23. doi: 10.1152/japplphysiol.01249.2001. [PubMed: 12133883]

59. Richardson A, Galvan V, Lin AL, Oddo S. How longevity research can lead to therapies for Alzheimer's disease: The rapamycin story. Exp Gerontol. 2015;68:51–8. doi: 10.1016/j.exger.2014.12.002. [PubMed: 25481271]

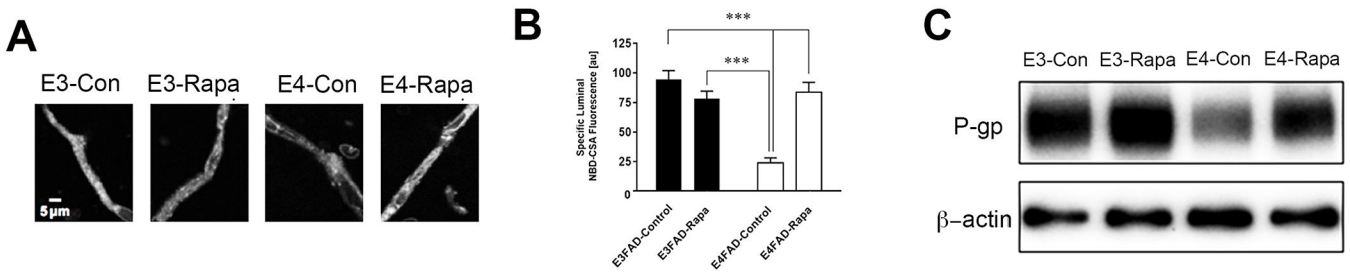

Figure 1. Effect of Rapamycin on the blood-brain barrier function and Aβ clearance.

(A) Representative confocal images showing decreased luminal accumulation of N-ε(4-nitro-benzofurazan-7-yl)-D-Lys(8)-cyclosporin A (NBD-CSA) fluorescence (white) in brain capillaries isolated from the old mice compared to young mice, indicating reduced P-glycoprotein (P-gp) activity. **(B)** Corresponding quantitative fluorescence data; images are shown in arbitrary fluorescence units (scale 0–255). **(C)** Western blotting (WB) for P-gp from the cortical vasculature, β-Actin was used as loading control. ***$p < 0.001$. Data are mean ± SEM.

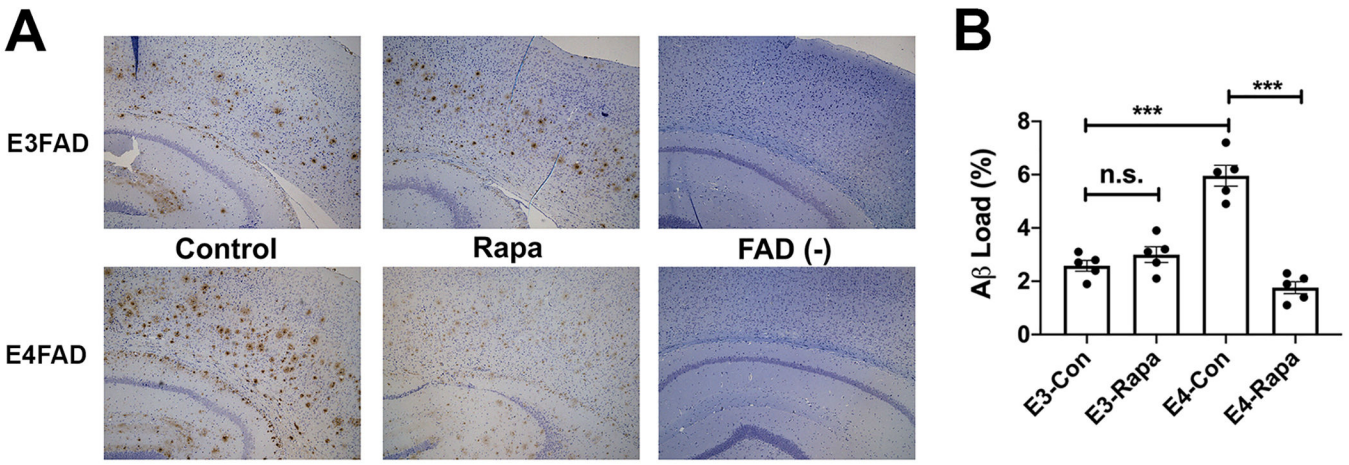

Figure 2. Effect of Rapamycin on Aβ retention.

(A) Representative images of Aβ immunohistochemical staining from the E3-control, E3-Rapa, E4-Control and E4-Rapa. The FAD negative brain tissue was used as controls to verify the Aβ loading. **(B)** quantitation of the Aβ load. Data are presented as the mean ± SEM. n.s. = not significant; ***$p < 0.001$.

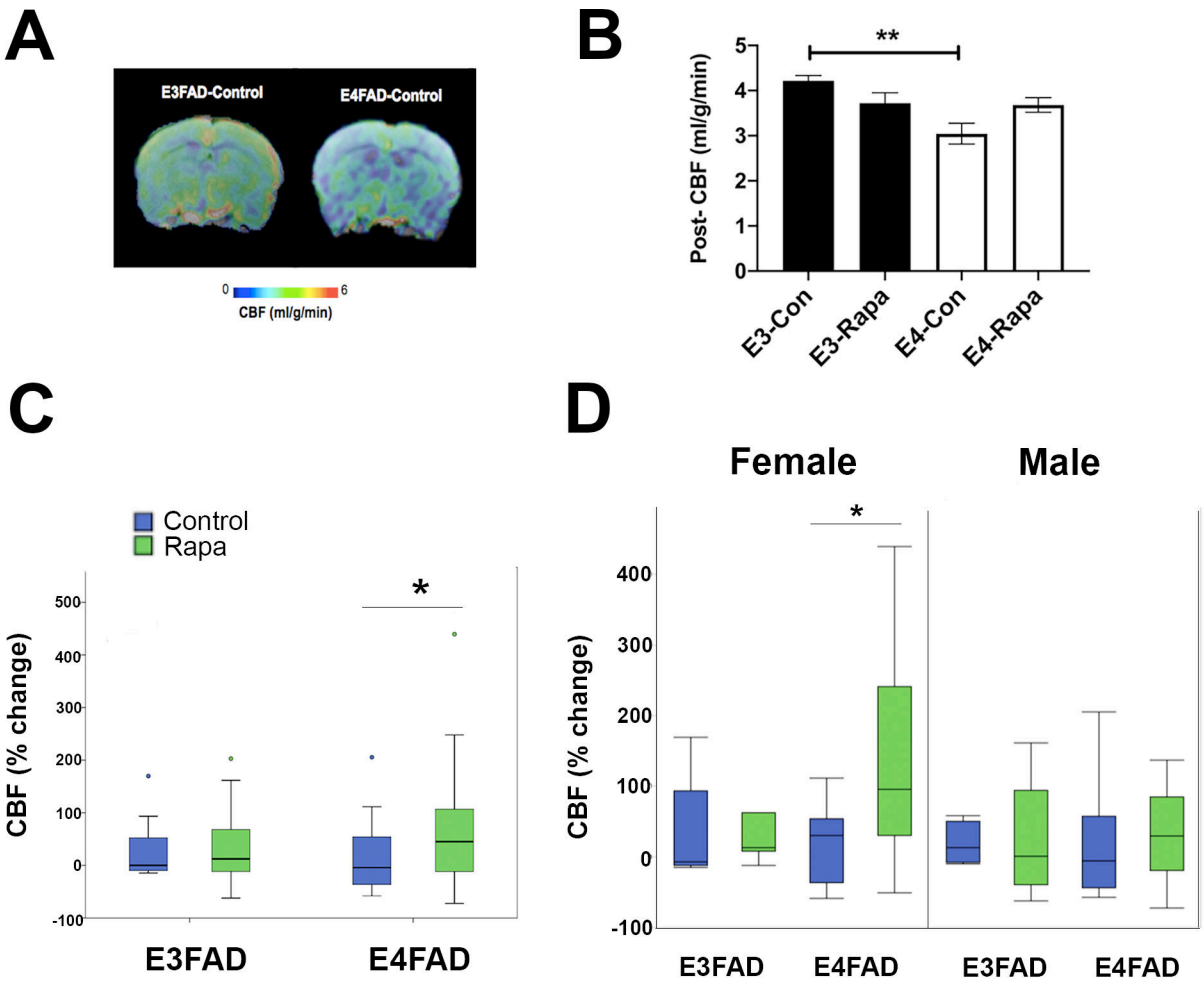

Figure 3. Cerebral blood flow (CBF) measurements.

(A) CBF images at 2 months of age; the color code indicates the level of CBF on a linear scale. (**B**) Post-treatment quantitative CBF (ml/g/min) obtained from hippocampus. (**C**) Pre- and post-treatment percent change in CBF for both E3FAD and E4FAD rapamycin fed mice. (**D**) Percent change in CBF stratified by sex. *$p < 0.05$; **$p < 0.01$. Data are mean ± SEM.

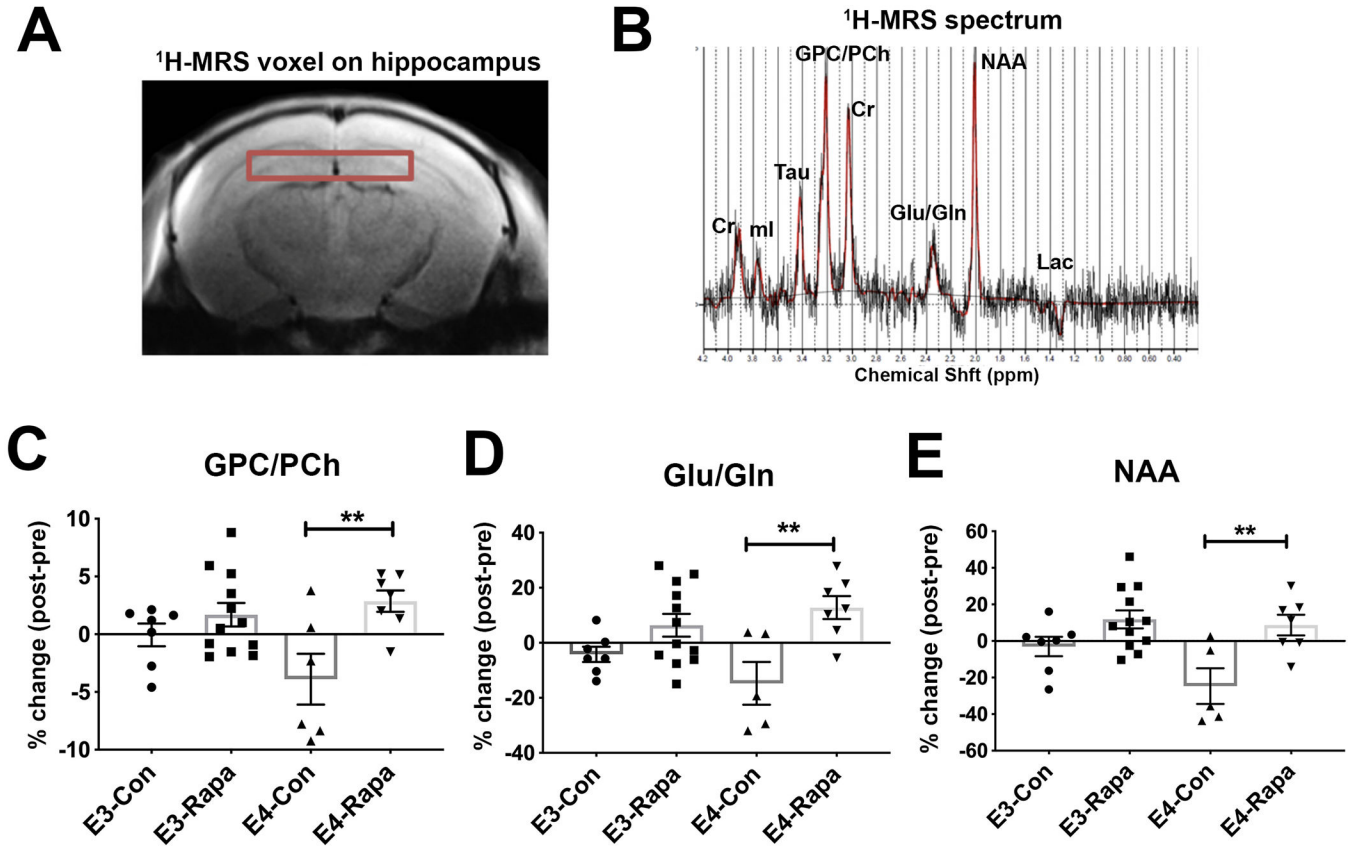

Figure 4. Brain metabolites determination *in vivo* using ^{1}H-MRS.

(A) The voxel replacement on the hippocampus and **(B)** the representative ^{1}H-MRS spectrum, showing lactate (Lac), N-acetyl-aspartate (NAA), glutamate (Glu) and glutamine (Gln), creatine (Cr), glycerophosphocholine (GPC) and phosphocholine (PCh), taurine (Tau) and myo-inositol (mI) in parts per million (ppm). Percent changes between pre-and post-treatment in **(C)** GPC and PCh, (**D**) Glu and Gln, and (**E**) NAA in E3-Control (E3-Con), E3-Rapa, E4-Control (E4-Con) and E4-Rapa groups. Data are Mean ± SEM. **p < 0.001.

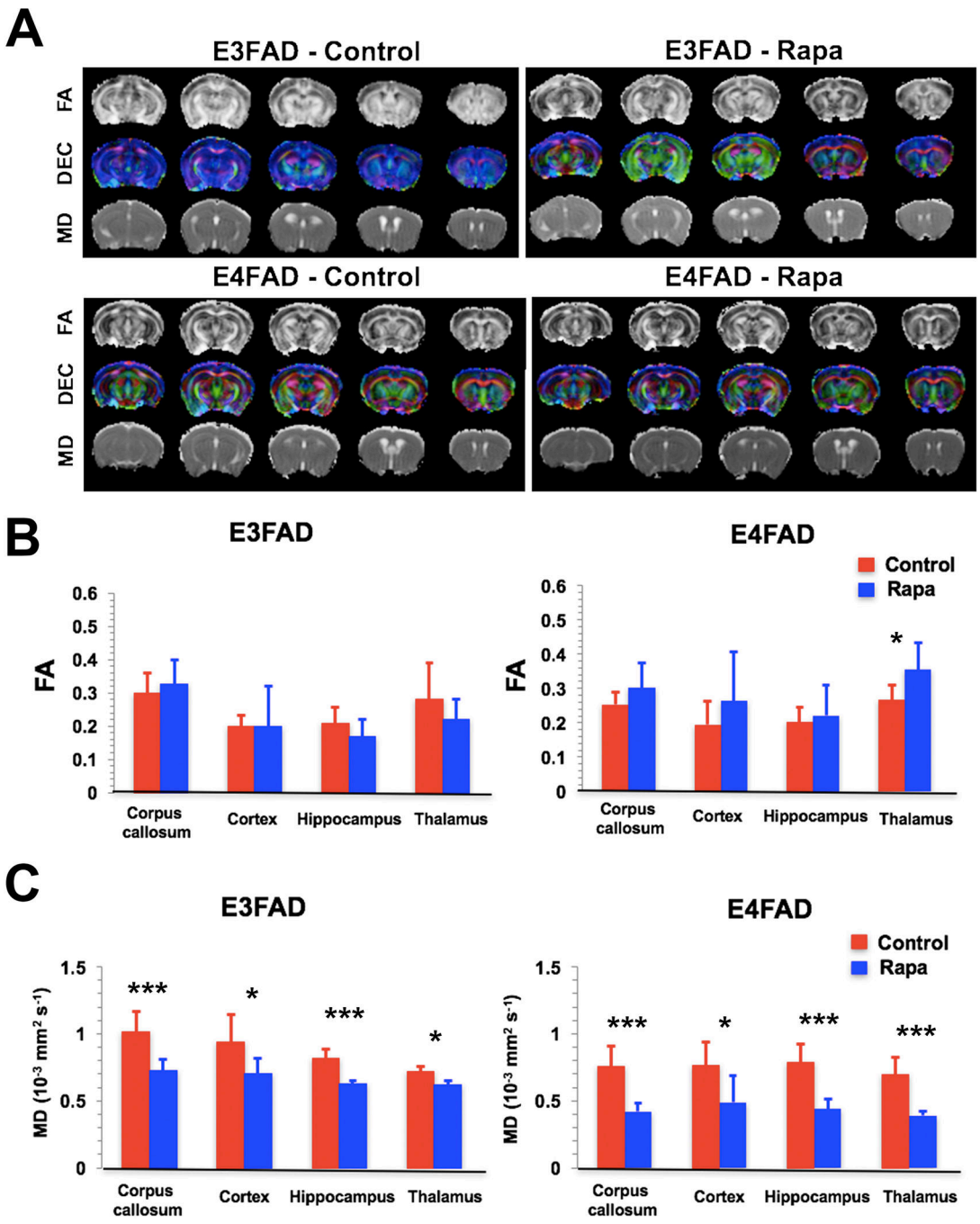

Figure 5. White matter integrity measurements.

(**A**) The maps showing fractional anisotropy (FA) and mean diffusivity (MD), and diffusion-encoded-color (DEC) of the four groups of mice. (**B**) Comparison of quantitative FA values in corpus callosum, cortex, hippocampus and thalamus between Control and Rapa groups. (**C**) Comparison of quantitative MD values in corpus callosum, cortex, hippocampus and thalamus between Control and Rapa groups. Data are Mean ± SEM. *p < 0.05. ***p < 0.0001.

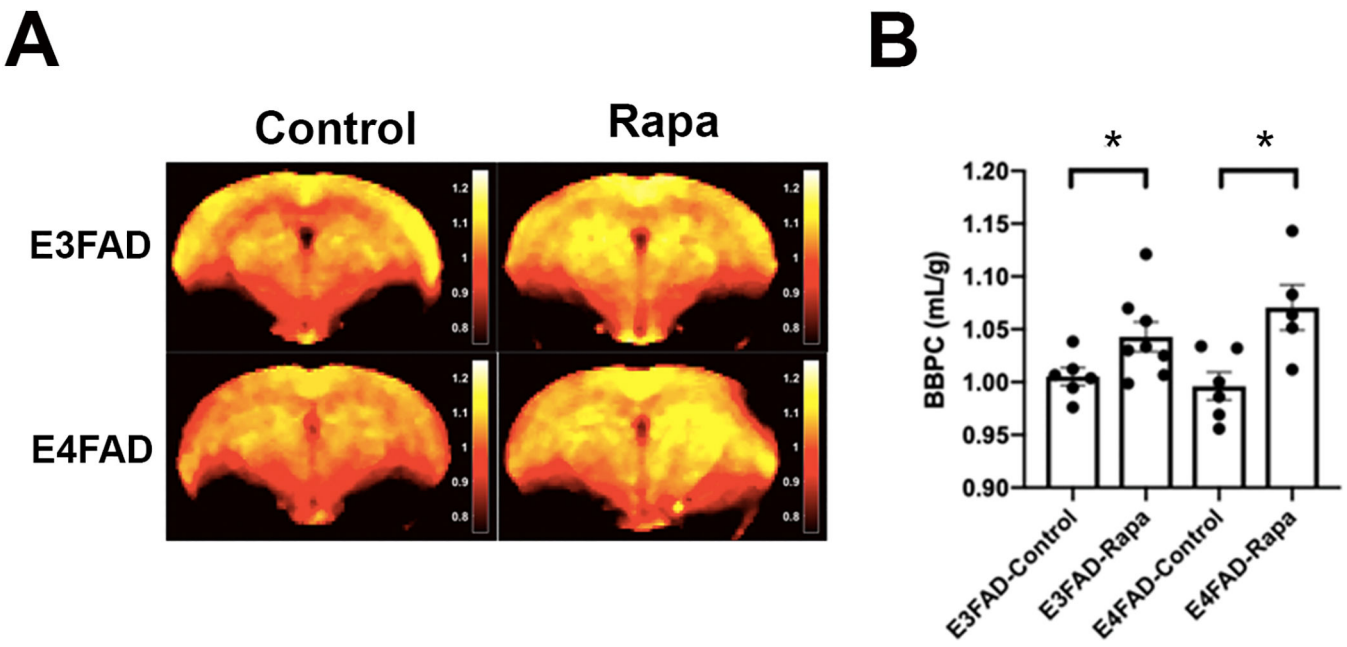

Figure 6. Water content measurements.

(**A**) Representative images of water content (indexed by BBPC) from each group. Yellow is representative of the highest water content, whereas red to black is low water content. **(B)** Mean and SEM for water content measured by brain-blood partition coefficient (BBPC). *$p < 0.05$.

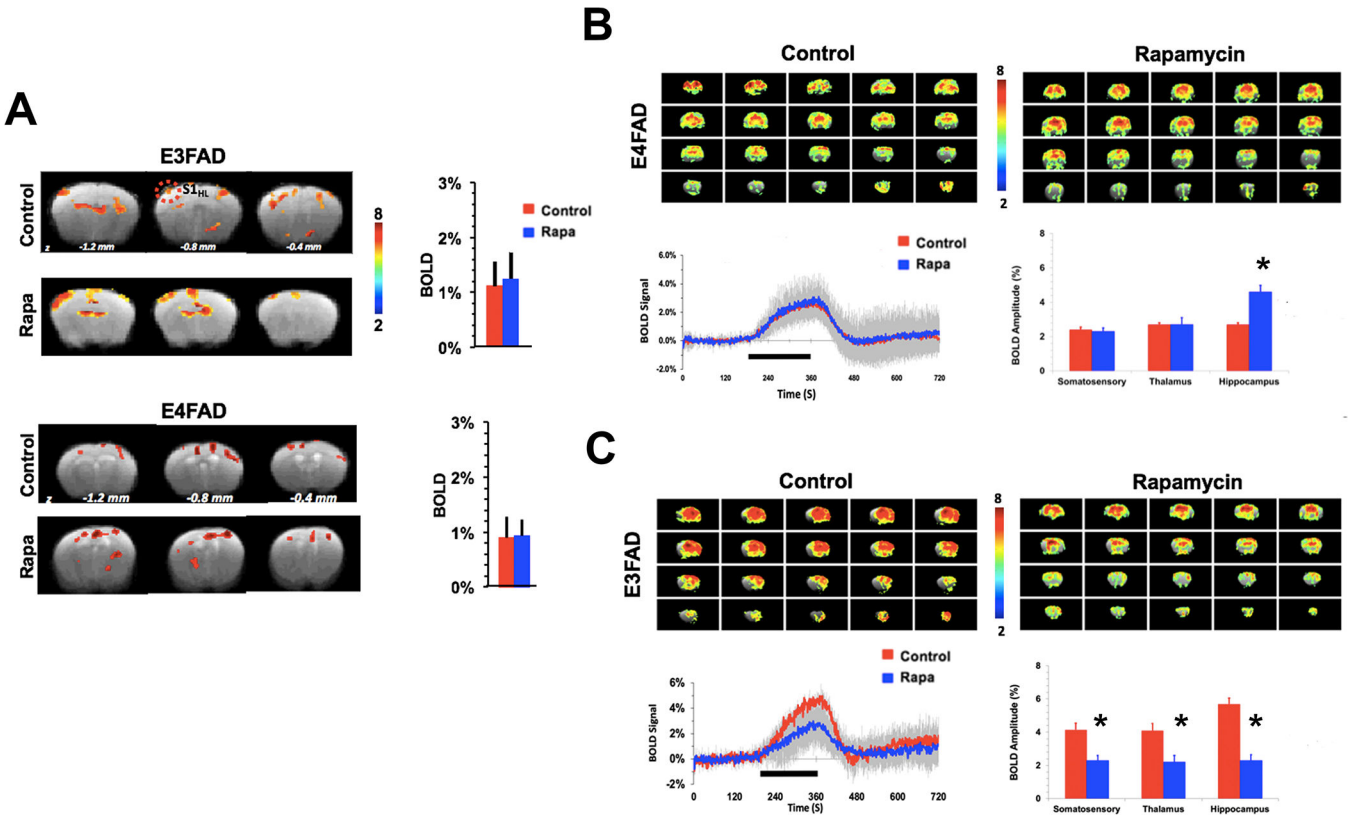

Figure 7. Hindpaw stimulation and cerebrovascular reactivity (CVR) responses.

(**A**) Maps (left) and percent of BOLD responses (right) under hindpaw stimulation in E3FAD and E4FAD mice. (**B**) (Top) CVR maps from the E4FAD-Control (left) and E4FAD-Rapa (right) mice; (Bottom left) an overall BOLD response curve between the two groups; (Bottom right) quantitative measures of CVR in somatosensory cortex, thalamus and hippocampus between the two group. (**C**) (Top) CVR maps from the E3FAD-Control (left) and E3FAD-Rapa (right) mice; (Bottom left) an overall BOLD response curve between the two groups; (Bottom right) quantitative measures of CVR in somatosensory cortex, thalamus and hippocampus between the two group. Data are Mean ± SEM. *p < 0.05.

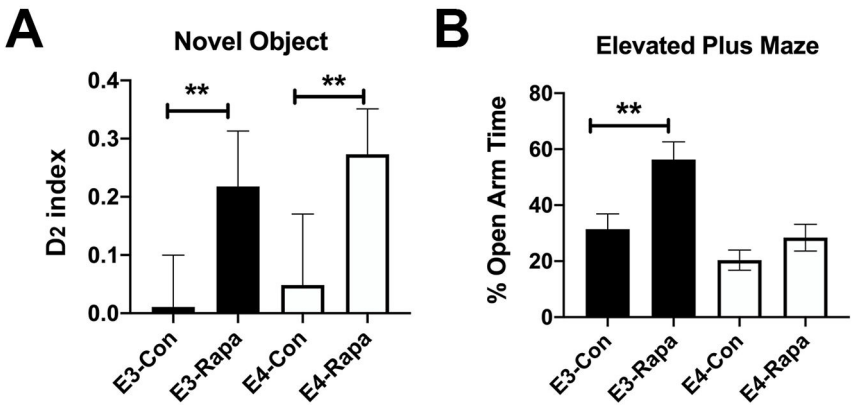

Figure 8. Behavior assessments in memory and anxiety.

(A) The Novel Object Recognition (NOR) test found the rapamycin-treated groups had a significantly higher recognition index, or D_2, than the control groups, independent of APOE-genotype. **(B)** The elevated plus maze (EPM) test found the E3FAD-Rapa mice had a significantly higher open arm duration compared to the E3FAD-control group; no differences were found between the E4FAD-Control and E4FAD-Rapa group. Data are Mean ± SEM. **$p < 0.01$.

Table 1.

Number for male and female mice in each experiment

Measurements	**# Male mice**		**# Female mice**	
	E3FAD	**E4FAD**	**E3FAD**	**E4FAD**
Cerebral blood flow (CBF)	8	8	8	8
Brain metabolites	8	8	8	8
Water content	6	6	6	7
White matter integrity	6	6	6	7
Cerebrovascular reactivity	6	5	6	7
Hindpaw stimulation	6	6	6	7
Behavioral tests	15	15	15	15
Blood-brain barrier function	6	18	6	18
Aβ staining	5	5	5	5
Brain tissue metabolomics	8	8	8	8

Table 2.

Study timeline and measurements.

Pre-treatment *in vivo* measurements (at 3 months of age)	Cerebral blood flow (CBF)
	Brain metabolites
Post-treatment *in vivo* measurements (at 7–8 months of age)	CBF
	Brain metabolites
	Water content
	White matter integrity
	Cerebrovascular reactivity
	Hindpaw stimulation
	Behavioral tests (NOR and EPM)
Postmortem biochemistry assays (at 7–8 months of age)	Blood-brain barrier function
	Aβ staining
	Brian tissue metabolomics

Table 3.

Rapamycin-induced brain free fatty acids metabolism changes in the E4FAD mice.

Changes of representative biochemicals involved in FFA metabolism between groups. Green represents $p \leq 0.05$ and group means fold change (FC) < 1.00.

Sub Pathway	Biochemical Name	Rapamycin Control	
		E3FAD	E4FAD
Long Chain Fatty Acid	margarate (17:0)	0.95	**0.79**
	oleate/vaccenate (18:1)	0.91	**0.78**
Polyunsaturated Fatty Acid (n3 and n6)	adrenate (22:4n6)	0.76	**0.51**
	dihomo-linoleate (20:2n6)	0.97	**0.63**
	mead acid (20:3n9)	0.90	**0.68**
	nisinate (24:6n3)	0.84	**0.66**

Table 4.
Rapamycin-induced brain glycolytic metabolism changes in the E3FAD mice.

Changes of representative biochemicals involved in glycolytic and carbohydrate metabolism between groups. Green represents $p \leq 0.05$ and group means fold change (FC) < 1.00.

Sub Pathway	Biochemical Name	Rapamycin Control	
		E3FAD	E4FAD
Glycolysis, Gluconeogenesis, and Pyruvate Metabolism	pyruvate	**0.77**	0.99
	lactate	**0.90**	0.95
	glycerate	**0.72**	0.86
TCA cycle intermediates	fumarate	**0.81**	1.01
	malate	**0.87**	1.02
Ketone bodies	3-hydroxybutyrate (BHBA)	**0.75**	0.91
Pentose Phosphate Pathway	ribulose 5-phosphate	**0.65**	0.77
	xylulose 5-phosphate	**0.56**	0.74
	ribose 1-phosphate	**0.57**	0.85
Pentose Metabolism	ribose	**0.88**	**0.91**
	ribitol	**0.84**	1.00
	ribonate	**0.87**	0.90
Fructose, Mannose and Galactose Metabolism	mannitol/sorbitol	**0.87**	1.02
	mannose-6-phosphate	**0.78**	0.72
Nucleotide Sugar	UDP-galactose	**0.81**	0.96
	UDP-N-acetylglucosamine/galactosamine	**0.80**	0.89
	cytidine 5’-monophospho-N-acetylneuraminic acid	**0.80**	**0.83**
Aminosugar Metabolism	N-acetyl-glucosamine 1-phosphate	**0.67**	0.83
	N-acetylneuraminate	**0.84**	0.92
	erythronate*	**0.88**	0.94

Table 5.

Pharmacogenetic differences between the E4FAD and E3FAD mice.

The measurements in comparison to control mice to measure the effects of rapamycin treated mice.

E4FAD-Rapa	E3FAD-Rapa
Normalized bodyweight	No change
Restored CBF, especially in females	
Restored brain metabolites related to neurotransmitters and neuronal integrity	
Restored BBB P-gp transporter quantity and Reduced Aβ retention	
Improved FA in Hippocampus	
Normalized free fatty acid level	Reduced glycolysis
No change	BOLD responses to CVR challenge
No change	Lower anxiety
Similar changes in the E3FAD-Rapa and E4FAD-Rapa mice	
Increased water content	
Improved cellularity (lower MD value)	
Enhanced recognition memory	
No change in hindpaw stimulation	